Multiscale numerical workflow describing microalgae motion and light pattern incidence towards population growth in a photobioreactor

Victor Pozzobon[1] ✉ **and Patrick Perré**[1]

[1]LGPM, CentraleSupélec, Université Paris-Saclay, SFR Condorcet FR CNRS 3417, Centre Européen de Biotechnologie et de Bioéconomie (CEBB), 3 rue des Rouges Terres 51110 Pomacle, France

In this article, a numerical workflow describing the microalgal growth inside of a photobioreactor is proposed. CFD is used to compute reactor internal hydrodynamics taking into account marine impeller rotation and sparged bubbles motion. Lagrangian approach is used to track microalgae motion inside of the culture vessel. The illumination across the reactor is obtained using the classical Beer-Lambert's law. The combination of light field and cell motion allows to reconstruct the light history of each microalgae. These histories are then supplied to Han's model which predicts individual growth rate and experienced photodamages. Once computed, several thousands of trajectories are agglomerated at the population level yielding the photobioreactor performances. After having ensured properties convergence, this procedure is applied to a large range of optical density (0 to 4.0), i.e. cell concentration, and incident light intensities (0 to 2 000 μmolPhoton/m^2/s). From this exploration, it is possible to determine the photobioreactor response surfaces in terms of growth rate and photodamages. These are latter used to propose an optimal lighting strategy for biomass production - reducing photobioreactor operation time by 16 % compared to classical two-step procedure - and assist light induced stress with the aim of triggering secondary metabolites production.

Photobioreactor | Growth | Light/dark cycles | Han's model | CFD

Correspondence: ***victor.pozzobon@centralesupelec.fr***

1. Introduction

Nowadays, microalgae are seen as a promising way to produces high added-value molecules such as pigments, essential fatty acids, specific carbohydrates, antioxidants (1). Being living organisms, triggering the desired molecules production usually requires a fine control over the culture. This culture commonly undergoes a two stage process: biomass production followed by a stress phase, inducing production of the molecule of interest (2).

In order to achieve the required level of control, the vessels are often closed and well regulated. pH, temperature and dissolved gases are usually set to desired fixed values through mechanical stirring or bubble induced mixing. Yet light patterns experienced by the cell cannot be made uniform. As microalgae are photosynthetic organisms, this may have an impact on their response to the culture protocol. As pointed by numerous authors, and reviewed by Abu-Ghosh (3), cells are being shuttled from high to low light intensity areas, and vice-versa. These light/dark cycles have been shown to have an important, adverse or beneficial, impact on algae growth. The most known effect being the flashing light effect - i.e. for a same total amount of light energy, growth can be promoted by taking advantage proper light/dark phases alternation (4–7).

Being able to assess the impact of this phenomena during the photobioreactor design stage would save both time and effort to engineers. That is why several attempts to acquire beforehand light/dark cycles have been led (8, 9). To do so, authors usually rely on computational fluid dynamics as it can yield tracers motion all around a reactor (10). For example, this was done to investigate the economical relevance of the addition of static mixer in tubular reactors (11, 12). The key parameters is usually the light/dark cycle frequencies. Sadly, few authors have linked cell positions - and experienced light patterns - to a proper microalgae growth model.

To do so, a cell level mechanistic model is required as pointed out by Bechet in his extensive review of light models predicting microalgal growth (13). This is the purpose of Han's model which links perceived illumination over time and cell growth. This approach also raises the question of the quality of the light field prediction. Improved methodologies have been delivered by some authors (14). Yet they used the obtained high quality light maps as input of averaged growth rate models. This highlights the complexity of properly predicting algae motion, experienced light/dark cycles and subsequent growth.

Nevertheless, this modeling approach has successfully been led for raceway open ponds (15), as light distribution inside of the vessel is obtained in a straightforward manner. Yet these reactors are usually placed outdoor, moderately controlled and do not offer as many ways to modify light/dark cycles as closed vessels. Applying the same approach to indoor photobioreactor is the aim of this work. Indeed, given the wide range of parameters one can control on this kind of reactor - aeration, stirrers speeds, external light intensity -, it would paves the way to improving the benefits drawn from the flashing light effect at the photobioreactor scale, as pointed out by Gao in his recent review (16). Among the few available studies, none produced a response surface of the

photobioreactor, nor dealt with impellers. Our work aims at boarding the community capabilities in these two aspects. As the first one is key for proper batch operation given the fact that the culture evolves with time. As for the second, it has been highlighted in recent work (17) that pneumatic mixing alone cannot achieve efficient flashing light effect. Indeed it restricts average achievable light/dark cycles frequencies and prevents the use of high diameter culture vessels because of low efficiency radial mixing.

In this work, the CFD-light-biological model coupling is applied to a 5 liter lab scale photobioreactor hosting a *Porphyridium sp.* culture (Fig. 1). The design is quite common: a cylindrical shape with a spherical lower end. Light is supplied externally by LEDs placed in an enclosure all around the reactor (not shown on the picture). CO_2-enriched air is bubbled by a cylindrical sparger to supply carbon to the culture. Stirring is ensured by a marine impeller. Finally, probes are immersed in the growth medium to allow for continuous monitoring. The whole system behavior is investigated numerically for different cell concentrations, light intensities and stirring speeds, to assess both growth and photodamages.

Fig. 1. Picture of the actual photobioreactor to be investigated

2. Mathematical model

In order to model the behavior of a whole photobioreactor, different submodels are coupled. First of all, a classical two phase flow model is used to predict internal hydrodynamic. Then, microalgae motion is tracked using Lagrangian approach. Illumination along the microalgae trajectories is obtained using cylindrical Beer-Lambert law. Finally, these information are supplied to Han's model in order to compute individual, and, by averaging, population growth rate.

2 1. Fluid dynamics model

The hydrodynamic features three different phases: the growth medium, considered as a continuum, the bubbles, considered as a dispersed gaseous phase and the microalgae considered as a dispersed solid phase. The dispersed phases are described as Lagrangian particles. They will be governed by the same equations, yet with different physical parameters.

2.1.1. Continuum description. The liquid flow is modeled using classical incompressible Navier Stokes equations, considering the growth medium as a Newtonian fluid. While valid for low concentration cultures, this assumption could be discussed for high density ones. Here, for the sake of simplicity, it will be maintained throughout this work. The stirrer motion is described using Multiple Reference Frame approach. This method approximates the rotary flow pattern around the impeller. To do so, the impeller shape is added to the case geometry, yet it will be kept stationary. Besides, a source term inducing a rotational flow is added into the Navier Stokes momentum equation (Coriolis force: $\alpha_s \rho_f \vec{\omega} \times \vec{u_f}$). This way, the main fluid structures can be reproduced. This approach is commonly used for the prediction of stirred tank hydrodynamics (18–20), provided the tank diameter is twice the one of the impeller (21). Its main advantage is to avoid the computation of a CPU intensive mesh deformation. In our case, a source term corresponding to a 100 rpm rotation speed is located in the volume in the vicinity of the impeller (where $\alpha_s = 1$ over 1.1 times the impeller diameter, 8 cm, 0 elsewhere). Furthermore, from a biological perspective, this rotation speed represents an impeller tip velocity of 0.64 m/s which is not harmful to *Porphyridium sp.* (damages being induced from 2.45 m/s (22)).

Bubbles are also contributing to the continuum motion. As they are traced using a Lagrangian approach (Sec. 2.1.2), the forces they apply on the liquid can directly be accounted for in the momentum balance equation ($\frac{1}{V_c}\sum_{i=1}^{n}\sum_{i=1}^{m}\vec{F_t^i}$).

In addition to the aforementionned phenomena, turbulence matters in the way the liquid moves around the reactor. In our case, the RNG-k-ϵ model is chosen to model it, as it proved to perform well in stirred tanks configurations (23–25). As fine computation of the shear stress induced pressure drop is not of interest here, walls interactions are described using high Reynolds approach, i.e. neglecting viscous sub-layer contribution.

Finally the continuum motion is governed by the following equation:

$$\begin{aligned}\frac{\partial}{\partial t}(\rho_f \vec{u_f}) + \nabla\cdot(\rho_f \vec{u_f}\vec{u_f}) = -\nabla p + \\ \nabla\cdot\left[(\mu+\mu_t)\left(\nabla\vec{u_f} + \nabla\vec{u_f}^{\,T}\right) - \frac{2}{3}\rho_f k\mathbf{I}\right] \\ - \frac{1}{V_c}\sum_{i=1}^{n}\sum_{i=1}^{m}\vec{F_t^i} - \alpha_s\rho_f\vec{\omega}\times\vec{u_f} + \rho_f\vec{g} \quad \textbf{(1)}\end{aligned}$$

Liquid properties are taken as those of 20 °C water (density: 998 kg/m^3, viscosity: 1.0 10^{-3} Pa.s, air-water surface tension: 72 mN/m).

2.1.2. Lagrangian phases description. Dispersed phases motion (bubbles and microalgae) is described using a La-

grangian approach. With this method the tracers trajectories are the results of a force balance. This balance sums the contribution of: virtual mass, drag and buoyancy (Eq. 2).

$$\rho_p V_p \frac{d\vec{u_p}}{dt} = \sum_{j=1}^{m} \vec{F_p^i} = -C_m \rho_f V_p \frac{d\vec{u_p}}{dt} + \frac{1}{2}\rho_f C_d S_p \|\vec{u_f} + \vec{u_t} - \vec{u_p}\|(\vec{u_f} + \vec{u_t} - \vec{u_p}) + V_p \vec{g}(\rho_f - \rho_p) \quad \textbf{(2)}$$

Where C_m is the virtual mass coefficient, C_d is the drag coefficient, and $\vec{u_t}$ the turbulent velocity fluctuation expressed as the two thirds of the square root of the turbulent kinetic energy supported by a randomly oriented ($\mathcal{U}[0, 4\pi]$) vector with a randomly drawn magnitude ($\mathcal{U}[0, 1]$) (Eq. 3).

$$\vec{u_t} = \frac{2}{3}\sqrt{k}\vec{\Lambda} \quad \textbf{(3)}$$

Potential tracers-walls collision are described using elastic shock model with no energy dissipation. The same description is used for cell-cell collisions. Bubble-bubble collisions are described with a 0.5 probability of coalescence provided their merging would yield a stable bubble (26). Furthermore, cells are considered spherical with a uniform diameter of 12 µm. Bubbles are also described as spherical as the sparger holes low diameter (0.5 mm) ensures the formation of small spherical bubbles. The bubble individual diameter is drawn from a Gaussian distribution, centered around 3.40 mm, the diameter that balance the sparger diameter using $2\pi R_s \sigma = \frac{4}{3}\pi R_b^3 g(\rho_f - \rho_b)$. The distribution standard deviation is taken as 10 % of the mean value. The coefficients describing the two Lagrangian populations are taken from literature and summarized in Table 1.

2.1.3. Case setup and solving strategy. The model is applied to the description of a 5 liter cylindrical photobioreactor with a spherical lower end. The culture volume inside of the reactor is 4.5 liters. This reactor features several key technical elements: a gas sparger, providing dissolved CO_2 to the microalgae, a marine impeller, preventing them from settling at the bottom of the bioreactor, a pH probe, allowing to monitor the culture online. In the numerical reproduction, the complex geometry induced by these elements is accounted for when meshing the culture volume. Figure 2 provides a schematic view of the numerical setup with the associated boundary conditions.

The CFD model is implemented under OpenFOAM (32) into an homemade solver. The code uses a PISO strategy (Pressure-Implicit with Splitting of Operators) to solve momentum and mass continuity equations. Momentum equation also features a two-way interaction with the bubbles swarm, as Langragian phase volume fraction is around 10^{-3} (33) (or below with around 100 bubbles present in the reactor at the same time). For every iteration, once the flow is computed, the bubbles and microalgae populations positions are updated. Mirocalgae positions are then extracted, associated

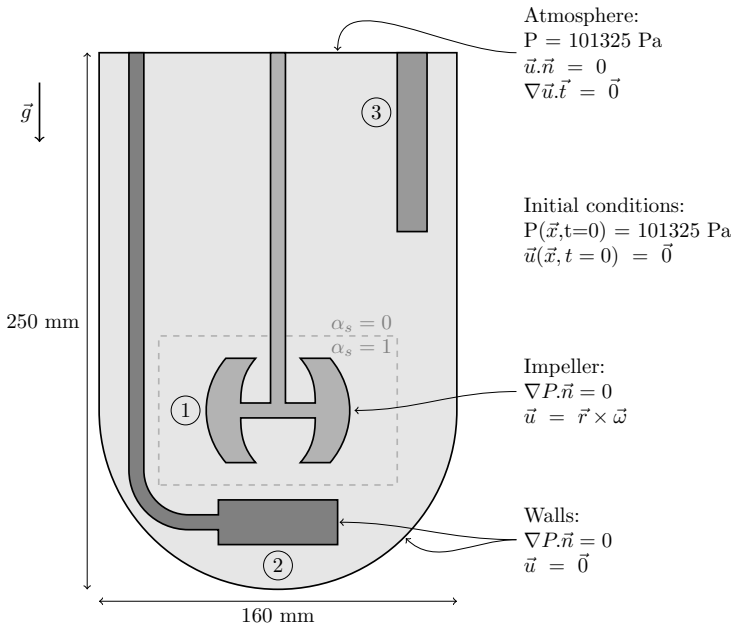

Fig. 2. Case geometry with initial and boundary conditions. Aeration: 0.1 vvm, stirring: 100 rpm. 1: stirred, 2: sparger, 3: pH probe. Dashed delimited: area where the momentum source term is applied to emulate stirrer motion

illumination and resulting growth are then computed. The mesh is made of about 200 000 cells, with a higher cell refinement near the walls and the solid elements immersed into the culture medium. Figure 3 provides a visualization of the numerical setup after 1 minute of run.

Being initially still, the water is set in motion by the marine impeller and the bubble motion. Yet after a certain time, the hydrodynamic enters into a quasi-steady state (see Appendix). The transient period should not be taken into account as it is only represent a tiny fraction (few seconds over a week) of the operation of an actual photobioreactor. Here, this timelap is around 10 seconds. In order to be conservative and to be sure that all the tracers trajectories would not feature artefacts from this transient state, the 60 first seconds are discarded. The code is then run for 10 minutes. Thus the total runtime is 11 minutes, which were produced in about 3 days on a desktop computer (3 threads, Intel(R) Xeon(R) CPU E5-2643 v3 @ 3.40GHz, DDR3 64 Go 2133MHz).

2 2. Light and cell growth model

Illumination field inside of the reactor is computed using the cylindrical Beer-Lambert law (34). Even though some authors have proposed corrections to this law, in order to take microalgae radiative properties into account (35), they have been shown to be a little influence for concentrated culture - the usual operating condition of a photobioreactor -, at least for cylindrical shapes (11). Thus, the unmodified law is used is this work (see Appendix).

From the CFD computation, the position of each tracer is extracted every 0.01 second (Fig. 4). Using the light field computed inside of the reactor, position and perceived illumination are linked for a given optical density (i.e. cell concentration). Because external lighting and cell concentration are

Table 1. Physical properties of the Lagrangian phases

	Symbol	Property	Ref.
Microalgae	ρ	1030 kg/m^3	(27)
	C_d	$\frac{24}{Re}(1+0.152Re^{0.677})+\frac{0.417}{1+5070Re^{-0.940}}$, Re < 2 10^5	(28)
	C_m	0.5, assumed to behave like solid spheres	-
	d	12 µm	(29)
Bubble	ρ	1.2 kg/m^3	-
	C_d	$\frac{24}{Re}(1+0.15Re^{0.687})$, Re < 1 000	(30)
	C_m	0.5	(31)
	d	Gaussian distributed (mean 3.40 mm)	-

Fig. 3. Visualization of the photobioreactor. Aeration: 0.1 vvm, stirring: 100 rpm. Lagrangian tracers: 10 000, only 100 represented (randomly drawn). Time: 1 minute. Color legend: blue - bubbles, red - tracers, orange - stirrer, yellow - sparger, purple - pH probe

assumed to have little impact on reactor hydrodynamic, this procedure can be repeated over a range of conditions. In this work, external light is considered uniform and ranges from 0 to 2 000 µmolPhoton/m^2/s, while optical density ranges from 0 to 4.0. The optical density is taken as the one that would yield a spectrophotometer mounted with 1.00 cm cuvettes.

Once light histories of all the tracers are built, the individual growth rate is computed using Han's model (Eq. 4, 5, and 6, Fig. 5). This model is now well-established in the community (36, 37) and has been shown to perform well given its low number of parameter (38). It links together perceived illumination (I) and resulting growth (B state and later µ) and photodamages (C state). In short (Fig. 5), it considers that open photosystems (A state) can convert light into chemicals, with a given photon capture chance (σ_{PSII}) and turnover rate ($1/\tau$). Yet if a processing photosystem is hit

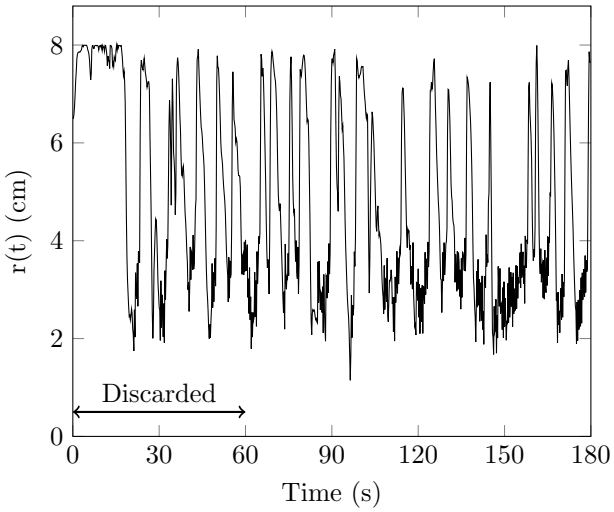

Fig. 4. Radial position of a randomly drawn tracer over the first 3 minutes of computation with a stirrer set at 100 rpm

before it returned to the open state, it may undergo damages (κ_d probability), that will later be repaired ($1/\kappa_r$ repair time). In our case, the parameters describing the cell responses are taken from previous work (39) (Tab. 2). It this work the parameters reproducing the light dependence of red marine algae *Porphyridium sp.* (UTEX637) were determinded using experimenal data (40) used as input to a particle swarm optimizer (39). For those experimental investigations, microalgae were grown under different light intensities, under different light/dark periods and fed with 3% CO_2 air bubbling. Thus, our numerical photobioreactor is performing the scale up of this strain under this level of CO_2. A point of note, should still be added, in this configuration, cells are considered as individuals. While true for the majority of growth conditions, this assumption can be invalidated under stress conditions. Indeed, as protection mechanism conferring a selective edge, cells can aggregate forming multicelluar stable bodies (41, 42). The possibility of cell clusters appearance under high light conditions cannot firmly be ruled out, still its investigation lies outside of the scope of this study.

$$\frac{dA}{dt} = -I\sigma_{PSII}A + \frac{B}{\tau} \quad \textbf{(4)}$$

$$\frac{dB}{dt} = I\sigma_{PSII}A - \frac{B}{\tau} + \kappa_r C - \kappa_d I\sigma_{PSII}B \quad \textbf{(5)}$$

$$\frac{dC}{dt} = \kappa_d I \sigma_{PSII} B - \kappa_r C \quad \textbf{(6)}$$

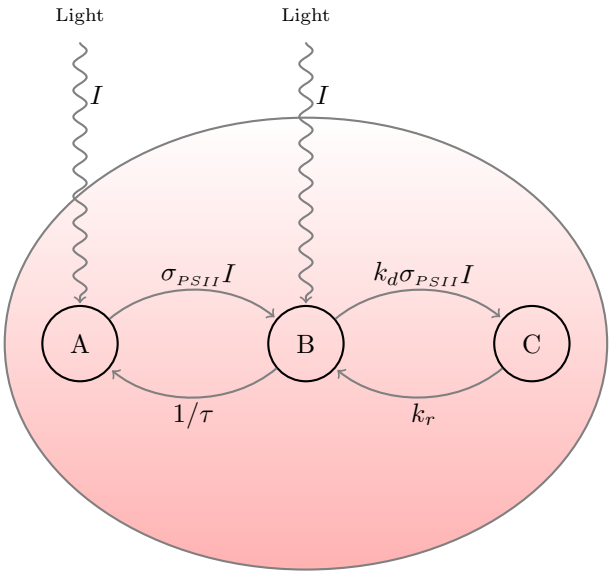

Fig. 5. Schematic representation of Han's model. Red ellipse: cell. Circle: photosystem. A: open state, B: processing state, C: photodamaged state (39)

Table 2. Han's model for *Porphyridium sp.* grown under 3 % CO2-enriched air (39, 40)

Parameter	Unit	Value
σ_{PSII}	m^2/µmolQuanta	3.85 10^{-3}
τ	s	2.81 10^{1}
κ_d	-	3.95 10^{-4}
κ_r	1/s	1.32 10^{-2}
K	s/h	8.57
Me	1/h	2.30 10^{-1}

The former equations system is integrated for every tracer at each time step. Thus it yields the fraction of open, working and damaged photosystems over the whole simulation. In order to go one step further, it is possible to link the photosystem state to population growth under the assumption that light is the limiting growth factor. With given units, i.e. μ in per hour, τ in seconds and Me in per hour, the equation governing population growth rate can be expressed as Eq. 7:

$$\mu = K\frac{B}{\tau} - Me \quad \textbf{(7)}$$

Still, in our case, Han's model calls for a comment. Indeed, cell physiological state may vary over the course a culture as they can manage their pigment content to either adapt low or excess light as well as redeploy nitrogen contained in chlorophylls. These variations could be taken into account through adaption of antenna size evolution (σ_{PSII}). In addition, cells can sometime aggregate. In this last condition, perceived light may be less for the inner cells than the outer ones. For the sake of simplicity, we considered cells as individuals with constant photosynthetic parameters.

Finally, individual growth rate are averaged into a population level growth rate. The integration procedure is repeated for each couple of light intensity and reactor optical density. In the end, it delivers the response surface of the microalgal population inside of the reactor over a wide range of incident light intensity and optical density.

3. Population level convergence

Before producing and commenting results at the photobioreactor scale, it is mandatory to ensure that the produced values are independent of purely numerical parameters. To do so, an increasing amount of tracer (from 1 to 10 000) is integrated over an increasing timelap (from 0.1 to 10 minutes). Population growth rates are computed for all those configurations. This test being computational power consuming, it is carried out for one operating condition: light intensity of 1 000 µmolPhoton/m^2/s and optical density of 1.0. The response surface is plotted in Figure 6. As one can see, the key numerical parameter is the integration time. Indeed, the number of tracer stops influencing the surface shape from few hundreds of tracers up to 10 000. Quantitatively, going from 3 000 integrated over 4.0 minutes, to 10 000 tracers integrated over 10 minutes conducts to a population growth rate variation below 1 %.

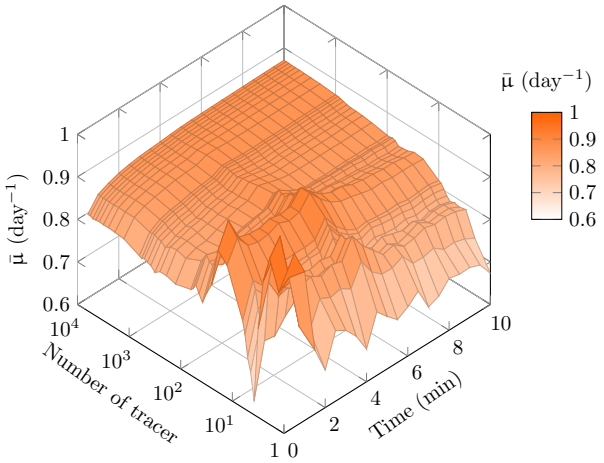

Fig. 6. Population level growth rate versus integration time and number of tracers. Optical density: 1.0. Light intensity: 1 000 µmolPhoton/m^2/s

From a computational perspective, the CPU-cost is born by the time integration. Increasing the number of integrated tracers has only a minimal effect. Convergence is led for this condition only (1 000 µmolPhoton/m^2/s and optical density of 1). Thus, in order to be conservative, 4 000 tracers were integrated over 5.0 minutes to produce all the coming results.

4. Results and discussion

4 1. Population level growth rate

Figure 7 (a) presents the population growth rate as a function of the incident light intensity and the culture optical density. As one can see, the population growth rate varies tremendously over the explored range of parameters. On the hand, it peaks at 1.35 day^{-1} for an optical density of 0.025 under 53 µmolPhoton/m^2/s. On the other hand, it can reach negative value in for high optical density, low illumination conditions,

delimited by the dashed line. This is in coherence with what is usually observed, the maximal growth happens for moderate light intensity and diluted cultures.

The general trends exhibited response surface can be explicated by combining mutual shading (or optical density) and photodamages (Fig. 7 (b)) concepts. At low incident illumination (e.g. below 50 µmolPhoton/m^2/s), light cannot trigger extensive photodamages (fraction of C state unit below 5 %), hence the effect of optical density is monotonic and decreasing. The sole shading effect explains the decreasing growth rate with increasing optical density. At moderate incident light (e.g. 500 µmolPhoton/m^2/s), photodamages dominate first (fraction of C state unit below 25 % for an OD of 0), as a low optical density means that light available everywhere in the photobioreactor at levels likely to trigger photodamages. Increasing the optical density allows then, at first, the averaged growth rate to increase, by mitigating photodamages. The growth rate then reaches a peak before the engaging a downward slope phase due to dominant effect of mutual shading. At high optical density (higher than 2.3), the growth rate eventually becomes negative. At large incident light (e.g. 1500 µmolPhoton/m^2/s), photodamages are generalized at low optical density and turns into an initial negative averaged growth rate. The optical density must increase significantly for the photodamages to be limited by mutual shading. Then, the growth rate follows a trend similar to the one at 500 µmolPhoton/m^2/s: peaking before decreasing. The decreasing rate is however much slower as the dark zones receive more light.

A point of note is the existence of a crest path for the maximal growth rate. Indeed, if one is to increase the incident light as the culture grows a high growth rate can be maintained over the photobioreactor operation. This crest path is represented by a solid black line in Figure 7. It starts from 1.35 day^{-1} (OD 0, light intensity 41 µmolPhoton/m^2/s) down to 0.82 day^{-1} for the maximum lighting conditions for an OD of 0.8. This crest path could probably continue further away as it stops when the maximum light intensity explored in this study is reached (2 000 µmolPhoton/m^2/s).

4 2. Constant optical density growth profile

Growing a culture at a given cell concentration (i.e. optical density) is a common procedure - refereed to as *turbidostat* or *PI curve* - to study the impact of light intensity on algal growth. Here, it is possible to extract this information at the photobioreactor scale. As example, an optical density of 1.0 is chosen. Figure 8 presents the growth for this optical density over the range of incident light intensities.

The culture exhibits three successive stages. From 0 to 600 µmolPhoton/m^2/s, the growth rate increases continuously, from negative values to about 0.85 day $^{-1}$. This stage corresponds to the affinity phase in which the higher the substrate - here light - the higher the growth rate. It is followed by a plateau phase over which the growth rate is somewhat constant between 95 and 100 % of its maximum value. Within this phase, the increase of photodamages undergone by the cells, when travelling in the most illuminated areas, is balanced by a larger amount of moderate light available in the shaded zones. This plateau comprises the light intensities from 500 to about 1600 µmolPhoton/m^2/s. Afterwards, the growth rate decreases as the light intensity increases. This last phase is the inhibition phase which sees a more and more important fraction of photodamaged cells.

This behavior is well-known (43, 44). The fact that the model is able to reproduce it as an emerging feature at the reactor scale using low level CFD and biological models is a token of its capabilities.

4 3. Comparison with static model

Another approach that is commonly used to predict photobioreactor performances is to average growth rates locally computed from the light field but without taking microalgae motion into account. This method is also referred as the second type of light model in (13). From this kind of growth models, the ones yielding to the best prediction are usually inverse of second order polynomial. This can be related to the fact that when on considered Han's model at steady state, the proportion of light processing photosystems follows this kind of law (Eq. 8).

$$B = \frac{I\sigma_{PSII}\tau}{1 + I\sigma_{PSII}\tau + \frac{\kappa_d}{\kappa_r}(I\sigma_{PSII})^2\tau} \qquad \textbf{(8)}$$

In order to better assess the importance of Lagrangian coupling, we compared the two methods (full Lagrangian coupling and static coupling) with the steady-state solution of Han's model (an imaginary photobioreactor with uniform light). Figure 9 reports the population growth rate obtained with these three assumptions under two different optical densities (0.2 (a) and 1.0 (b)). The first comment is that using the incident light intensity as sole guide is unadvisable. Indeed, cylindrical geometries concentrate light on their axis, which is not taken into account by this simplistic approach. The second approach is more sucessful, at least for the low optical density. In this case, this approach captures the trend and is close to absolute values delivered by Han's model coupled with CFD. This can be explained by the fact that light is available in the whole reactor. Hence hydrodynamic has only a minor impact. This illustrates what was pointed out by biologists who pioneered the study of photosynthesis at the population scale: illumination has to be homogeneous throughout the reactor in order to access the intrinsic cell response (45, 46). On the opposite, this approach fails to predict reactor performances at higher optical densities. This points out one important feature of algal growth: the time characteristic of photodamages. In the case of a static reactor, cells experience the same light intensity over time. Photodamages therefore completely develop in the highly illuminated zones and growth is completely inhibited in dark zones. For this reason, applying a Han' model without Lagrangian pathways cannot be predictive. Still it could account for the influence of internal hydrodynamics provided the parameters used in Eq. 8 are adjusted, which is a common procedure. Yet, in this case, the model loses its predictive capabilities as these parameters would have to be calibrated again for any change of the

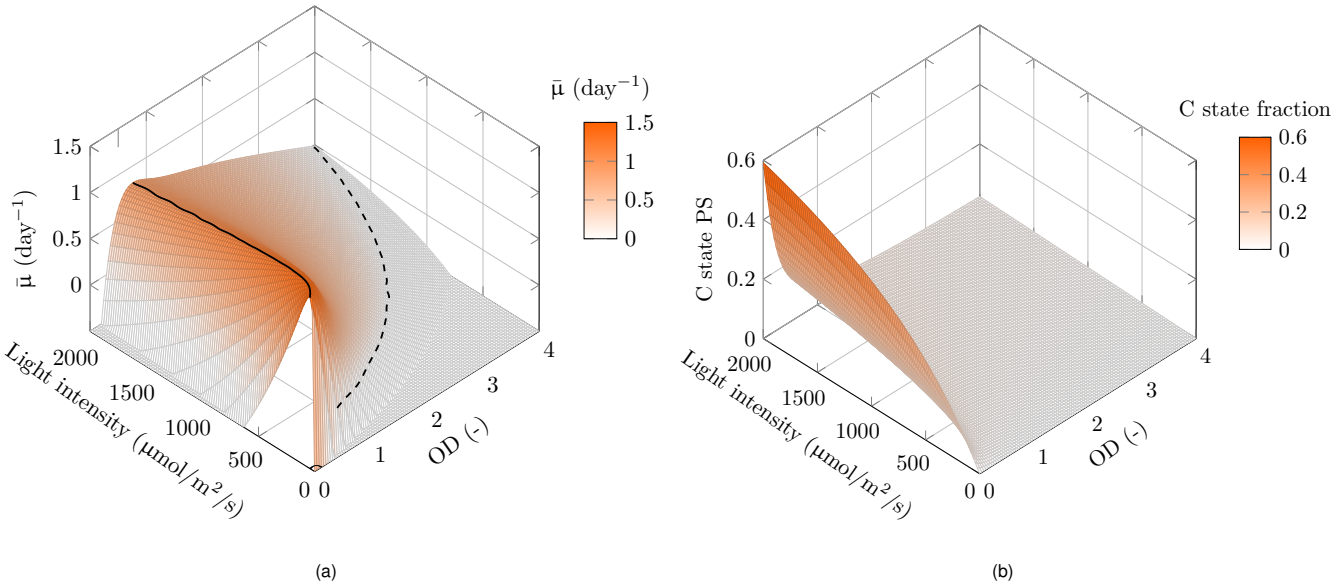

(a) (b)

Fig. 7. Population level growth rate (a) and experienced photodamages (b) versus optical density and incident light intensity. Continuous line: growth rate crest path. Dashed line: null growth rate. Number of tracer: 4 000. Integration time: 5.0 minutes

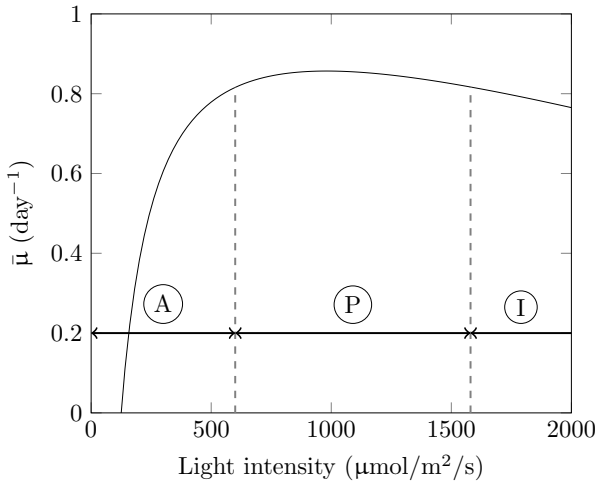

Fig. 8. Population level growth at a given optical density and varying incident light intensity. Optical density: 1.0. A: affinity phase, P: plateau phase, I: inhibition phase. Number of tracer: 4 000. Integration time: 5.0 minutes

culture conditions (geometry, volume, aeration, stirring...). This comments highlighting the added-value of CFD combined Han's model in the prediction of emerging behaviour at the bioreactor level.

4 4. Optimal lighting strategy

From the obtained response surface, it is possible to envision an optimal operation procedure for the reactor with the aim of shortening biomass production time. Indeed following the maximum growth crest path would lower the time required to reach the maximal biomass concentration.

Two configurations are compared.

- the first one is a culture growing along the crest path until it reaches 2 000 μmolPhoton/m^2/s. At this point, the light intensity is set constant to this maximum value.
- the second culture is grown under 500 μmolPhoton/m^2/s until it reaches an optical density of 1.0. Then, the lighting is set at 2 000 μmolPhoton/m^2/s. The second strategy is what could be done experimentally in order to speed up the growth process, it is referred to as the two steps strategy hereinafter. Even though not optimal, this procedure is not a naive one nonetheless. Indeed, this protocol can be derived from the operation of the reactor as a turbidostat at an optical density of 1.0. This would yield Figure 8 results. From them, the operator could conclude that switching light from 500 to 2 000 μmolPhoton/m^2/s at an optical density of 1.0 would yield the same growth rate and allow the culture to cope well with high lighting intensity.

Both cultures are starting at an optical density of 0.05.

The two predicted scenarii are reported in Figure 10. As one can see, both cultures have similarities: a linear growth phase during which they achieve the same daily productivity (calculated between 10 and 90 %, using the following correlation: Optical Density = 0.4777 × Dry Weight (47)) and the same final optical density. This is normal given the fact that the culture is light limited. With the same final amount of light cast over the reactor, the final cell concentration is bound to be the same in both cases. The main difference between two cultures is the lag phase and the subsequent time needed to reach the final concentration. In the case of the optimal lighting strategy, the growth time (to reach 90 % of the final cell concentration) is 5.5 days while it is 6.4 days in the two step light strategy.

The determination of the crest path, hence the optimal lighting strategy seems almost impossible experimentally while it is rather easy numerically. Yet this mode of operation yields subsequent benefits: it is less energy intensive and time consuming. From an experimental perspective, following the numerically determined growth rate crest path can easily be achieved. Indeed, it would require the driving the

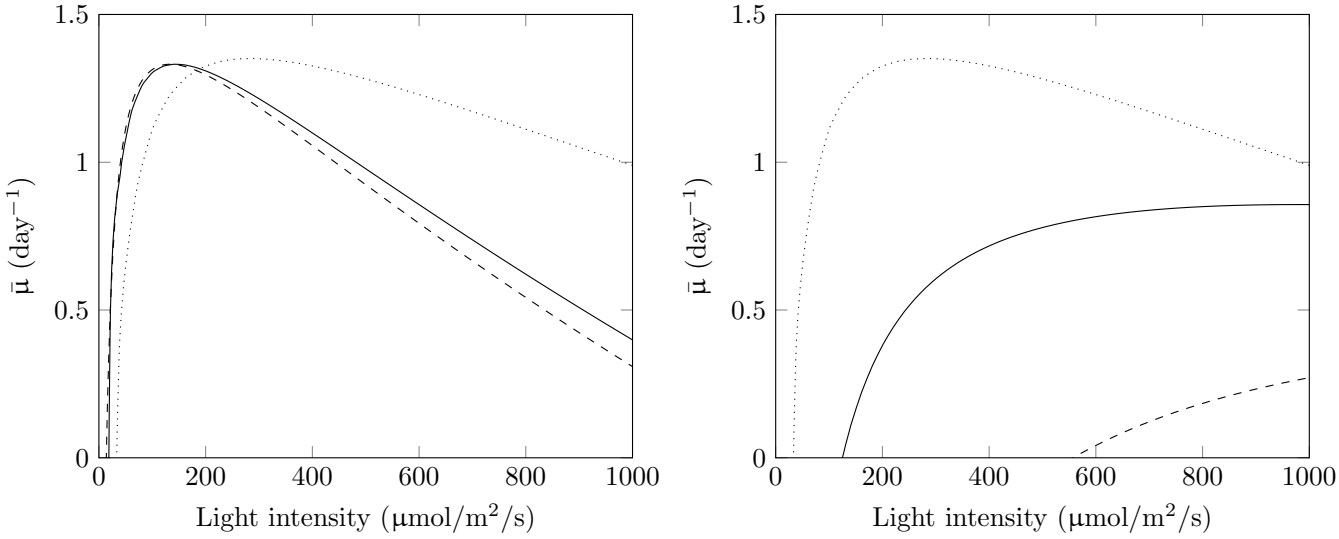

Fig. 9. Population level growth rate at versus incident light intensity, at an OD of 0.2 (a) and 1.0 (b). Solid line: taking cells motion into account, dashed line: Han's model applied locally without taking microalgae motion into account, doted line: Han's model applied only using incident light intensity and without taking microalgae motion into account

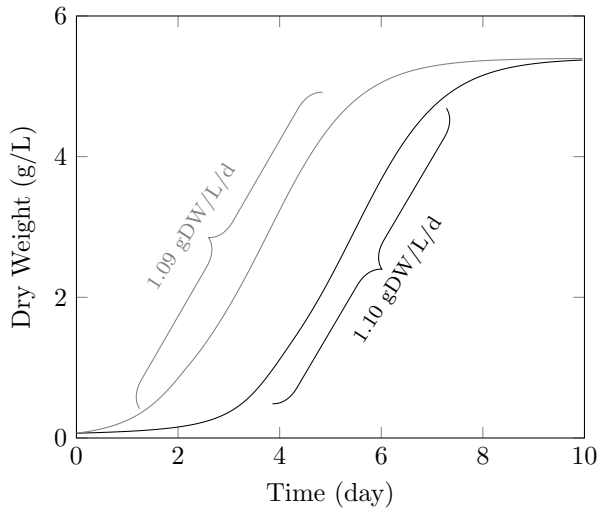

Fig. 10. Predicted microalgal density inside of the reactor. Black line: two steps lighting strategy - 500 µmolPhoton/m^2/s until an optical density of 1.0 is reached, 2 000 afterwards -. Gray line: optimal lighting strategy. Initial optical density: 0.05 / Initial dry weight: 0.1 g/L

light source by the reading of an immersed optical density probe.

4 5. Culture stress

Another possibility offered by the numerical tool is the determination of a light stress zone in the photobioreactor operating conditions. This can be of interest as light stress, in combination with nitrogen limitation or even starvation, is used to trigger high added-value secondary metabolites production by mircoalgae. Here, Han's model yields the amount of photodamaged photosystems, thus this quantity can also be plotted as a surface response (Fig. 7 (b)). As one could have expected, the highest amount of photodamages is achieved for low optical densities, high illumination conditions.

Combining the growth and photodamages response surfaces could yield an operation procedure that would first promote biomass production before triggering secondary metabolites production, through light excess. Yet this may turn out to be challenging. Indeed, it would have to be done by carefully choosing the initial amount of nitrogen in the medium (not accounted for in this study) and anticipating cell pigment composition evolution during the second phase. Furthermore, these operating conditions modifications are likely to induce a variation in cells response to light which would have to be incorporated in the cell biological model. In any case, the proposed numerical workflow would be of help in limiting the time that would require sole experimental approach.

Finally, the proposed numerical can be used to derive some insights about the influence of the stirring speed over induced light stress. Indeed, this parameter can have two opposite effects. On the one hand lowering the stirring speed would allow the cell to spend more time in light intense areas, increasing the amount of experienced photodamages. On the other hand, increasing the stirring speed would lower individual photodamages, yet increase the number of cells experiencing those damages by shuttling more microalgae towards the reactor walls. To investigate theses effects, another numerical trial is produced setting the stirrer speed at 50 rpm. Figure 11 presents population level photodamages at the maximum light intensity (2 000 µmolPhoton/m^2/s) for the two stirring speeds. Higher stirring speed provides higher intensity photodamages of the whole population, this for both low and high optical densities. This can be explained by the fact that the characteristic time triggering photodamages is shorter than the recovering one. Hence shuttling cells in the highly illuminated zone results in a higher level of photodamages at the culture level. For minimal optical density, the two stirring speeds provide the same damage intensity - around 0.6 -. It is normal given the fact that the culture is translucent

and this the photobioreactor is fully illuminated. From this in can be concluded that when stressing a culture, reducing the stirrer speed is not an efficient strategy.

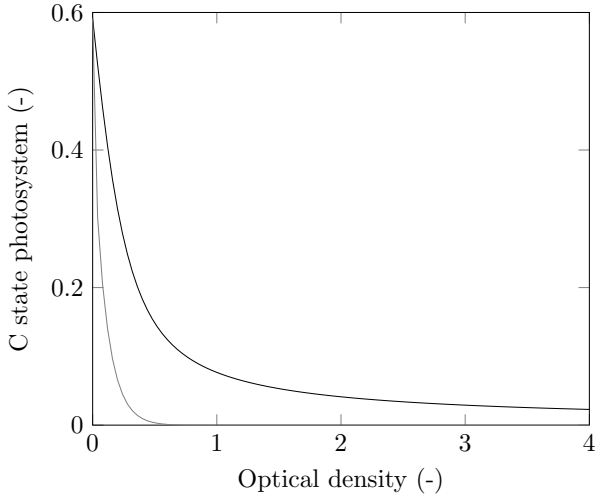

Fig. 11. Fraction of the photodamaged photosystems at the population level. Light intensity: 2 000 μmolPhoton/m^2/s. Black line: stirrer set at 100 rpm. Gray line: stirrer set at 50 rpm

5. Conclusion

In this article a numerical workflow describing the microalgal growth inside of a photobioreactor is proposed. This tools computes reactor internal hydrodynamics and uses it to track microalgae motion inside of the culture vessel. The illumination across the reactor is obtained using classical Beer-Lambert's law. Afterwards, light histories of the cell are built before being supplied to Han's model. Individual growth rate and experienced photodamages are computed and agglomerated at the population level.

Hence population growth can be computed at the reactor scale. A range of optical density, i.e. cell concentration, and incident light is explored, assuming cell intrinsic response to light does not change with those two parameters. From this exploration, it is possible to determine the photobioreactor response surfaces in terms of growth rate and photodamages. These are latter used to propose an optimal lighting strategy for biomass production - reducing photobioreactor operation time by 16 % compared to classical two-step procedure - and assist light induced stress with the aim of triggering secondary metabolites production.

There are two main possibility of improvement of this work. First, by taking into the evolution of cell response to light with ageing of the culture (e.g. cell pigment content management), or different physiological states (light and/or nitrogen stressed). Second, by confronting models prediction with the actual operation of a photobioreactor.

Declaration of author contributions & conflict of interest

PP and VP initiated and designed the study together. VP ran the computations. PP and VP critically interpretative the results. VP drafted the manuscript, PP corrected it. Both authors equally contributed to this work and approve the manuscript.

The authors have no conflict of interest to declare.

References

1. Muhammad Rizwan, Ghulam Mujtaba, Sheraz Ahmed Memon, Kisay Lee, and Naim Rashid. Exploring the potential of microalgae for new biotechnology applications and beyond: A review. *Renewable and Sustainable Energy Reviews*, 92:394–404, September 2018. ISSN 1364-0321. .
2. Imran Pancha, Kaumeel Chokshi, Basil George, Tonmoy Ghosh, Chetan Paliwal, Rahulkumar Maurya, and Sandhya Mishra. Nitrogen stress triggered biochemical and morphological changes in the microalgae Scenedesmus sp. CCNM 1077. *Bioresource Technology*, 156: 146–154, March 2014. ISSN 0960-8524. .
3. Said Abu-Ghosh, Dror Fixler, Zvy Dubinsky, and David Iluz. Flashing light in microalgae biotechnology. *Bioresource Technology*, 203:357–363, March 2016. ISSN 0960-8524. .
4. Jörg Degen, Andrea Uebele, Axel Retze, Ulrike Schmid-Staiger, and Walter Trösch. A novel airlift photobioreactor with baffles for improved light utilization through the flashing light effect. *Journal of Biotechnology*, 92(2):89–94, December 2001. ISSN 0168-1656. .
5. Carsten Vejrazka, Marcel Janssen, Mathieu Streefland, and René H. Wijffels. Photosynthetic efficiency of Chlamydomonas reinhardtii in flashing light. *Biotechnology and Bioengineering*, 108(12):2905–2913, 2011. ISSN 1097-0290. .
6. Shi-Kai Wang, Amanda R. Stiles, Chen Guo, and Chun-Zhao Liu. Microalgae cultivation in photobioreactors: An overview of light characteristics. *Engineering in Life Sciences*, 14(6): 550–559, November 2014. ISSN 1618-2863. .
7. Wendie Levasseur, Behnam Taidi, Robin Lacombe, Patrick Perré, and Victor Pozzobon. Impact of seconds to minutes photoperiods on Chlorella vulgaris growth rate and chlorophyll a and b content. *Algal Research*, 36:10–16, December 2018. ISSN 2211-9264. .
8. Luca Giannelli, Hideki Yamaji, and Tomohisa Katsuda. A Numerical Model for the Quantification of Light/Dark Cycles in Microalgal Cultures: Air-Lift and Bubble-Column Photobioreactor Analysis by Means of Computational Fluid Dynamics. *JOURNAL OF CHEMICAL ENGINEERING OF JAPAN*, 48(1):61–71, January 2015. ISSN 0021-9592. .
9. Toru Sato, Daiki Yamada, and Shinichiro Hirabayashi. Development of virtual photobioreactor for microalgae culture considering turbulent flow and flashing light effect. *Energy Conversion and Management*, 51(6):1196–1201, June 2010. ISSN 0196-8904. .
10. J. P. Bitog, I. B. Lee, C. G. Lee, K. S. Kim, H. S. Hwang, S. W. Hong, I. H. Seo, K. S. Kwon, and E. Mostafa. Application of computational fluid dynamics for modeling and designing photobioreactors for microalgae production: A review. *Computers and Electronics in Agriculture*, 76(2):131–147, May 2011. ISSN 0168-1699. .
11. Chao Qin and Jing Wu. Influence of successive and independent arrangement of Kenics mixer units on light/dark cycle and energy consumption in a tubular microalgae photobioreactor. *Algal Research*, 37:17–29, January 2019. ISSN 2211-9264. .
12. Iris Perner-Nochta and Clemens Posten. Simulations of light intensity variation in photobioreactors. *Journal of Biotechnology*, 131(3):276–285, September 2007. ISSN 0168-1656. .
13. Quentin Béchet, Andy Shilton, and Benoit Guieysse. Modeling the effects of light and temperature on algae growth: State of the art and critical assessment for productivity prediction during outdoor cultivation. *Biotechnology Advances*, 31(8):1648–1663, December 2013. ISSN 0734-9750. .
14. Ezequiel Franco-Lara, Jan Havel, Frank Peterat, and Dirk Weuster-Botz. Model-supported optimization of phototrophic growth in a stirred-tank photobioreactor. *Biotechnology and Bioengineering*, 95(6):1177–1187, 2006. ISSN 1097-0290. .
15. Philipp Hartmann, David Demory, Charlotte Combe, Raouf Hamouda, Anne-Céline Boulanger, Marie-Odile Bristeau, Jacques Sainte-Marie, Bruno Sialve, Jean-Philippe Steyer, Sophie Rabouille, Antoine Sciandra, and Olivier Bernard. Growth Rate Estimation of algae in Raceway Ponds: A novel Approach. *IFAC Proceedings Volumes*, 47(3): 6216–6221, January 2014. ISSN 1474-6670. .
16. Xi Gao, Bo Kong, and R. Dennis Vigil. Simulation of algal photobioreactors: recent developments and challenges. *Biotechnology Letters*, 40(9):1311–1327, October 2018. ISSN 1573-6776. .
17. Giovanni Luzi, Christopher McHardy, Christoph Lindenberger, Cornelia Rauh, and Antonio Delgado. Comparison between different strategies for the realization of flashing-light effects – Pneumatic mixing and flashing illumination. *Algal Research*, 38:101404, March 2019. ISSN 2211-9264. .
18. D. A. Deglon and C. J. Meyer. CFD modelling of stirred tanks: Numerical considerations. *Minerals Engineering*, 19(10):1059–1068, August 2006. ISSN 0892-6875. .
19. Allan Wang, Zhihui Xiao, and Hamid Ghazialam. Evaluation of the Multiple Reference Frame (MRF) Model in a Truck Fan Simulation. SAE Technical Paper 2005-01-2067, SAE International, Warrendale, PA, May 2005.
20. W. Bujalski, Z. Jaworski, and A. W. Nienow. CFD Study of Homogenization with Dual Rushton Turbines—Comparison with Experimental Results: Part II: The Multiple Reference Frame. *Chemical Engineering Research and Design*, 80(1):97–104, January 2002. ISSN 0263-8762. .
21. Lanre Oshinowo, Zdzislaw Jaworski, Kate N. Dyster, Elizabeth Marshall, and Alvin W. Nienow. Chapter 35 - Predicting the tangential velocity field in stirred tanks using the Multiple Reference Frames (MRF) model with validation by LDA measurements. In H. E. A. van den Akker and J. J. Derksen, editors, *10th European Conference on Mixing*, pages 281–288. Elsevier Science, Amsterdam, January 2000. ISBN 978-0-444-50476-0. .
22. T. Mazzuca Sobczuk, F. García Camacho, E. Molina Grima, and Yusuf Chisti. Effects of agitation on the microalgae Phaeodactylum tricornutum and Porphyridium cruentum. *Bioprocess and Biosystems Engineering*, 28(4):243, October 2005. ISSN 1615-7605. .
23. B. Zakrzewska and Z. Jaworski. CFD Modeling of Turbulent Jacket Heat Transfer in a Rush-

ton Turbine Stirred Vessel. *Chemical Engineering & Technology*, 27(3):237–242, 2004. ISSN 1521-4125. .
24. M. Ammar, W. Chtourou, Z. Driss, and M. S. Abid. Numerical investigation of turbulent flow generated in baffled stirred vessels equipped with three different turbines in one and two-stage system. *Energy*, 36(8):5081–5093, August 2011. ISSN 0360-5442. .
25. J Aubin, D. F Fletcher, and C Xuereb. Modeling turbulent flow in stirred tanks with CFD: the influence of the modeling approach, turbulence model and numerical scheme. *Experimental Thermal and Fluid Science*, 28(5):431–445, April 2004. ISSN 0894-1777. .
26. Grace J. R, Wairegi T, and Nguyen T. H. Shapes and velocities of single drops and bubbles moving freely through immiscible liquids. | Article Information | J-GLOBAL. *Trans Inst Chem Eng*, 54(3):167–173, 1976. ISSN 0046-9858.
27. F. Fasaei, J. H. Bitter, P. M. Slegers, and A. J. B. van Boxtel. Techno-economic evaluation of microalgae harvesting and dewatering systems. *Algal Research*, 31:347–362, April 2018. ISSN 2211-9264. .
28. Brown Phillip P. and Lawler Desmond F. Sphere Drag and Settling Velocity Revisited. *Journal of Environmental Engineering*, 129(3):222–231, March 2003. .
29. M. del Pilar Sánchez-Saavedra, Fátima Y. Castro-Ochoa, Viridiana Margarita Nava-Ruiz, Duahmet A. Ruiz-Güereca, Ana Laura Villagómez-Aranda, Fabián Sigueiros-Vargas, and Ceres A. Molina-Cárdenas. Effects of nitrogen source and irradiance on Porphyridium cruentum. *Journal of Applied Phycology*, 30(2):783–792, April 2018. ISSN 1573-5176. .
30. Akio Tomiyama, Isao Kataoka, Iztok Zun, and Tadashi Sakaguchi. Drag Coefficients of Single Bubbles under Normal and Micro Gravity Conditions. *JSME International Journal Series B Fluids and Thermal Engineering*, 41(2):472–479, May 1998. ISSN 1340-8054, 1347-5371. .
31. C. D. Ohl, A. Tijink, and A. Prosperetti. The added mass of an expanding bubble. *Journal of Fluid Mechanics*, 482:271–290, May 2003. ISSN 1469-7645, 0022-1120. .
32. Hrvoje Jasak, Aleksandar Jemcov, and Željko Tuković. OpenFOAM: A C++ Library for Complex Physics Simulations. 2007.
33. S. Elghobashi. On predicting particle-laden turbulent flows. *Applied Scientific Research*, 52 (4):309–329, June 1994. ISSN 1573-1987. .
34. Tomohisa Katsuda, Takeshi Arimoto, Koichi Igarashi, Masayuki Azuma, Jyoji Kato, Susumu Takakuwa, and Hiroshi Ooshima. Light intensity distribution in the externally illuminated cylindrical photo-bioreactor and its application to hydrogen production by Rhodobacter capsulatus. *Biochemical Engineering Journal*, 5(2):157–164, June 2000. ISSN 1369-703X. .
35. F. G. Acién Fernández, F. García Camacho, J. A. Sánchez Pérez, J. M. Fernández Sevilla, and E. Molina Grima. A model for light distribution and average solar irradiance inside outdoor tubular photobioreactors for the microalgal mass culture. *Biotechnology and Bioengineering*, 55(5):701–714, 1997. ISSN 1097-0290. .
36. BO-PING HAN. Photosynthesis–Irradiance Response at Physiological Level: a Mechanistic Model. *Journal of Theoretical Biology*, 213(2):121–127, November 2001. ISSN 0022-5193. .
37. BO-PING HAN. A Mechanistic Model of Algal Photoinhibition Induced by Photodamage to Photosystem-II. *Journal of Theoretical Biology*, 214(4):519–527, February 2002. ISSN 0022-5193. .
38. Paul Rudnicki, Xi Gao, Bo Kong, and R. Dennis Vigil. A comparative study of photosynthetic unit models for algal growth rate and fluorescence prediction under light/dark cycles. *Algal Research*, 24:227–236, June 2017. ISSN 2211-9264. .
39. Victor Pozzobon and Patrick Perre. Han's model parameters for microalgae grown under intermittent illumination: Determined using particle swarm optimization. *Journal of Theoretical Biology*, 437:29–35, January 2018. ISSN 0022-5193. .
40. Xiaoxi Wu and Jose C. Merchuk. A model integrating fluid dynamics in photosynthesis and photoinhibition processes. *Chemical Engineering Science*, 56(11):3527–3538, June 2001. ISSN 0009-2509. .
41. William C. Ratcliff, R. Ford Denison, Mark Borrello, and Michael Travisano. Experimental evolution of multicellularity. *Proceedings of the National Academy of Sciences*, 109(5): 1595–1600, January 2012. ISSN 0027-8424, 1091-6490. . Publisher: National Academy of Sciences Section: Biological Sciences.
42. MARTIN E. Boraas, DIANNE B. Seale, and JOSEPH E. Boxhorn. Phagotrophy by a flagellate selects for colonial prey: A possible origin of multicellularity. *Evolutionary Ecology*, 12 (2):153–164, February 1998. ISSN 1573-8477. .
43. Hugh L. MacIntyre, Todd M. Kana, Tracy Anning, and Richard J. Geider. Photoacclimation of Photosynthesis Irradiance Response Curves and Photosynthetic Pigments in Microalgae and Cyanobacteria1. *Journal of Phycology*, 38(1):17–38, February 2002. ISSN 1529-8817. .
44. Richard J. Geider, Hugh L. MacIntyre, and Todd M. Kana. A dynamic regulatory model of phytoplanktonic acclimation to light, nutrients, and temperature. *Limnology and Oceanography*, 43(4):679–694, 1998.
45. Bessel Kok. Chapter 6. In *Algal culture from laboratory to pilot plant.*, pages 63–75. Carnegie Institute Washington Pub, 1953.
46. J. Neal Phillips and Jack Myers. Growth Rate of Chlorella in Flashing Light. 1. *Plant Physiology*, 29(2):152–161, March 1954. ISSN 0032-0889.
47. Hu-Ping Luo and Muthanna H. Al-Dahhan. Airlift column photobioreactors for Porphyridium sp. culturing: Part I. effects of hydrodynamics and reactor geometry. *Biotechnology and Bioengineering*, 109(4):932–941, 2012. ISSN 1097-0290. .

Appendix

Transient timelap assessment

The time required to reach the quasi-steady state is an important parameter of this study. Indeed, the photobioreactor is operated for a long time. Hence only quasi-steady state is

Latin symbols

A	open state photosystem, -
a	absorptivity, -
B	processing state photosystem, -
C	damaged state photosystem, -
C_d	drag coefficient, -
C_m	virtual mass coefficient, -
d	diameter, m
$\vec{F}$	force, N
g	gravity acceleration, 9.81 m/s^2
I	light intensity, µmolPhoton/m^2/s
K	growth rate conversion factor, s/h
K_a	absorption coefficient, 1/m
k	turbulent kinetic energy, m^2/s^2
l	length, m
Me	maintenance rate, 1/h
P	pressure, Pa
Q	flow rate, m^3/s
R	radius, m
Re	Reynolds number, -
r	radial position, m
S	surface, m^2
t	time, s
$\vec{t}$	tangeantial vector, -
$\mathcal{U}$	uniform distribution, -
$\vec{u}$	velocity vector, m/s
$\vec{x}$	position vector, m
z	length, m

Greek symbols

α	phase indicator for Coriolis force, -
θ	angle, rad
κ	repair/damage rate, 1/s
µ	growth rate, 1/day
μ	dynamic viscosity, Pa.s
ρ	density, kg/m^3
σ	photosystem absorption cross section, m^2/µmolPhoton
τ	processing time, s
$\vec{\omega}$	rotation vector, rad/s

Subscripts

0	initial, at (t,z) = 0
b	bubble
c	mesh cell
d	damage
f	fluid
i	tracer index
j	force index
m	force total number
n	tracer total number
$PSII$	PhotoSystem II
p	particle
r	repair
s	sparger
t	turbulence
z	at a length z

Superscripts	
T	transpose

Other symbols	
.	dot product
$\times$	cross product
∇	nabla operator, 1/m
$\vec{a}$	vector notation
$\bar{a}$	population quantity
$\mathbf{I}$	identity matrix

Table 3. Nomenclature

relevant, the transient time lap should be discarded. To assess for this time, volume averaged momentum inside of the reactor is monitored (Fig. 12). Volume averaged momentum gets stable after about 10 seconds.

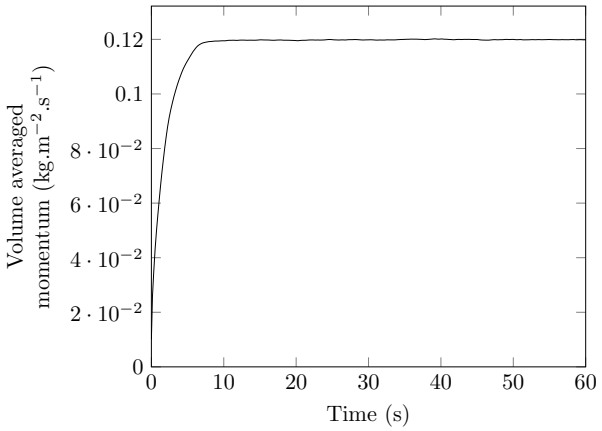

Fig. 12. Volume averaged momentum. Aeration: 0.1 vvm, stirring: 100 rpm

Cylindrical Beer-Lambert law

Figure 13 presents a graph supporting the computation of the illumination at a given radial position inside of a cylindrical photobioreactor. For a given position, light rays comes from a 2π angle (Eq. 9). Yet the distance they travel from the reactor walls varies, hence the amount of attenuation the are submitted to. As a consequence, the wall point distance has to be computed for each step of the integral (Eq. 10).

$$I(r) = \int_0^{2\pi} I_0 exp(-K_a l(r,\theta)) d\theta \quad \textbf{(9)}$$

$$l(r,\theta) = r cos\theta + \sqrt{R^2 - r^2 sin^2\theta} \quad \textbf{(10)}$$

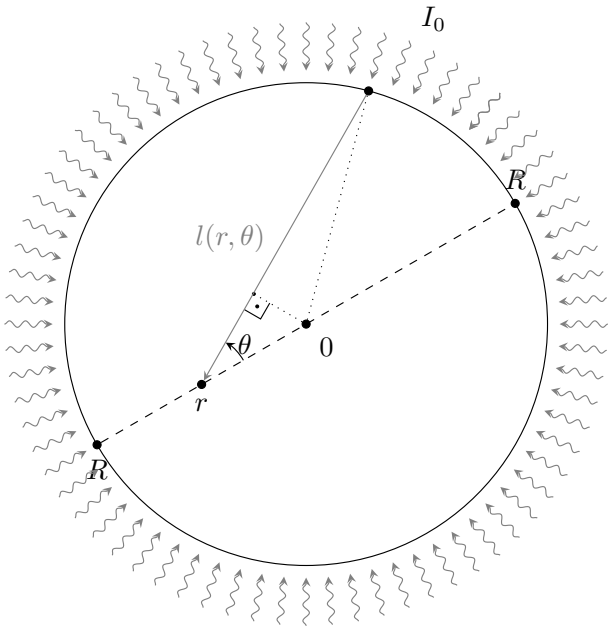

Fig. 13. Light attenuation in a cylindrical geometry